Robotica (2016) volume 34, pp. 383–402. © Cambridge University Press 2014
doi:10.1017/S0263574714001520

Tri-pyramid Robot: stiffness modeling of a 3-DOF translational parallel manipulator

Qiang Zeng*, Kornel F. Ehmann and Jian Cao

Department of Mechanical Engineering, Northwestern University, 2145 Sheridan Road, Evanston, IL 60208-3111, USA

(Accepted May 19, 2014. First published online: June 20, 2014)

SUMMARY

This paper presents a 3-DOF (degree of freedom) translational parallel manipulator named the Tri-pyramid Robot. Compared to the developed 3-DOF translational parallel manipulators, the Tri-pyramid Robot is designed based on conical displacement subset to exhibit better kinematic characteristic. The inverse position solution is obtained through closed-loop constraint analysis and used to formulate the overall Jacobian matrix of constraints and actuations based on the theory of reciprocal screws. Furthermore, by considering the stiffness of all links, joints, actuators, fixed, and moving platforms, the output stiffness matrix of the Tri-pyramid Robot is derived by the transformations of loads and deformations in the closed-loop form. The relations between the virtual input-output displacements are analyzed by the overall Jacobian matrix and used to build the manipulator's stiffness model. Stiffness performance is evaluated by the extreme eigenvalues of the output stiffness matrix in the reachable workspace. By considering the variations of the structural parameters and the distribution of the output stiffness, the maximal stiffness workspace is obtained through numerical optimization, providing, thereby, basic constraints for the parametric design of the Tri-pyramid Robot.

KEYWORDS: Parallel manipulator; Mechanism design; Stiffness matrix; Theory of reciprocal screws.

Nomenclature

$O_f - x_f y_f z_f$ — fixed reference frame
$O_m - x_m y_m z_m$ — moving reference frame
R — revolute joint
P — prismatic joint
Co_i — constraint cone surface
Z_m — output motions of the moving platform
$\{R(\boldsymbol{n_{i,j}})\}$ — a rotation around vector $\boldsymbol{n_{i,j}}$
$\{T(\boldsymbol{l_i})\}$ — a translation along vector $\boldsymbol{l_i}$
$\{T(Co_i)\}$ — two translations on cone surface
$\{T\}$ — three orthogonal translations
$\{X(\boldsymbol{n_i})\}$ — Schoenflies motion
$\{Co(\boldsymbol{n_{i,j}}, Co_i)\}$ — conical displacement subset
$\alpha_i, \alpha_{Pi}, \alpha_{Ri}, \gamma_i, \|\boldsymbol{r_i}\|, \|\boldsymbol{h_{i,u}}\|, \|\boldsymbol{h_{i,d}}\|$ — basic structural parameters
$\theta_{i,u}, \theta_{i,d}, \|\boldsymbol{h_i}\|$ — variables of passive joints
$\|\boldsymbol{l_i}\|$ — input variables of actuated joints
$\boldsymbol{r_O}$ — output variable of the moving platform
$\boldsymbol{\omega}$ — angular velocity of the moving platform

* Corresponding author. E-mail address: qiangzengnu@gmail.com

https://doi.org/10.1017/S0263574714001520 Published online by Cambridge University Press

$\boldsymbol{v}$ — linear velocity of the moving platform
$\$_{\boldsymbol{Om}}$ — instantaneous twist of the moving platform
$\hat{\$}_{i,j}$ — unit screw associated with the j^{th} joint of the i^{th} subchain
$\boldsymbol{s}_{i,j}$ — unit vector that is along the j^{th} joint axis of the i^{th} subchain
$\hat{\$}_{i,c}$ — unit constraint screw
$\hat{\$}_{i,a}$ — unit actuation screw
$\boldsymbol{k}_{i,c}$ — unit constraint vector
$\boldsymbol{k}_{i,a}$ — unit actuation vector
∇ — transformation matrix
$\boldsymbol{J}_{\boldsymbol{c}}$ — Jacobian of constraints
$\boldsymbol{J}_{\boldsymbol{a}}$ — Jacobian of actuations
$\boldsymbol{J}$ — overall Jacobian matrix
$\boldsymbol{f}_{i,a}$ — actuation force
$\boldsymbol{M}_{i,c}$ — constraint couple
$C_{i,j}$ — compliance of link
$\tau_{i,a}$ — torque of actuator
$K_{i,\alpha a}$ — torsional stiffness of actuator
$\Delta\alpha_{i,a}$ — angular deformation of actuator
$d_{i,a}$ — pitch diameter of lead screw
$L_{i,a}$ — lead of lead screw
$\lambda_{i,a}$ — lead angle of lead screw
$\psi_{i,a}$ — friction angle of lead screw
$\alpha_{i,t}$ — radial angle of thread
$\mu_{i,c}$ — coefficient of friction between screw and nut
Δl_i — linear displacement of slide block
$\Delta\varphi_{i,j}$ — angular deformation of link
E — Young's modulus of elasticity
$I_{ik,j}$ — moment of inertia of area
$K_{i,al}$ — stiffness of actuations
$K_{i,c}$ — stiffness of constraints
$\boldsymbol{f}_{\boldsymbol{f}}$ — output force
$\boldsymbol{M}_{\boldsymbol{f}}$ — output torque
$\boldsymbol{w}_{\boldsymbol{f}}$ — output wrench
$\boldsymbol{\Delta O}_{\boldsymbol{m}}$ — deformations of the moving platform
$\boldsymbol{\Delta l}$ — translational deformations of the actuators
$\boldsymbol{\Delta}\varphi_{\boldsymbol{c}}$ — rotational deformations of constrained subchains
$\boldsymbol{K}_{\boldsymbol{f}}$ — stiffness matrix of the Tri-pyramid Robot
$K_{f\max}$ — maximal eigenvalues of the stiffness matrix
$K_{f\min}$ — minimal eigenvalues of the stiffness matrix

1. Introduction

3-DOF (degree of freedom) Translational Parallel Manipulators (TPMs) have been developed in many different forms.[1–14] There are three typical 3-DOF TPMs, namely, the Delta Robot,[1,2] the Tsai mechanism,[3–7] and the Cartesian parallel manipulator.[8–14] These designs have been used in many practical applications including manufacturing, medical, and food industries to mention a few. However, the developed 3-DOF TPMs still suffer from a variety of drawbacks. The structural disadvantage of the Delta Robot is its complex structure with a total of 21 1-DOF joints. The Tsai mechanism includes six universal joints, and the three actuators are not placed on the fixed platform. Cartesian parallel manipulators have orthogonally arranged constraints and, furthermore, the actuation force of each subchain independently resists the external force. All of the above-mentioned characteristics lead to low stiffness and accuracy of these parallel manipulators. In order to overcome their drawbacks, this paper presents and analyses a 3-DOF TPM call the "Tri-pyramid Robot."

For precision manipulation purposes, the structural stiffness is an important performance measure. In order to evaluate the stiffness distribution in the workspace of a parallel manipulator, its stiffness

https://doi.org/10.1017/S0263574714001520 Published online by Cambridge University Press

model should be established in the form of an output stiffness matrix. As far as the stiffness modeling of parallel manipulators is concerned, there are many research works that have been developed. Gosselin[15] analyzed the stiffness of parallel manipulators based on the Jacobian matrix. The method was extended by taking into account the stiffness of the actuators and links.[16] Lumped modeling was used based on the expansions of the traditional rigid model by adding virtual joints, which described the elastic deformations of the manipulator's components by lumped parameters. El-Khasawneh and Ferreira[17] established the minimal and maximal stiffness in an arbitrary direction for the Stewart Platform, and the stiffness map was used in machine tool design. Ceccarelli and Carbone[18] deduced the stiffness matrix of the Cassino Parallel Manipulator. A numerical investigation was carried out on the effects of the design parameters by using the determinant of the stiffness matrix as a stiffness performance index. Huang *et al.*[19] presented a simple yet comprehensive approach for the stiffness modeling of a tripod-based parallel machine. Their work was further developed by Xi *et al.*[20]

More recently, Zhang and Lang[21] analyzed the stiffness model of reconfigurable parallel kinematic machines based on the Jacobian matrix and lumped modeling. Pham and Chen[22] presented the stiffness model based on flexure members that were connected together in serial or parallel combinations. The functional relationships between the stiffness and dimensions as well as the free shape of a 3-DOF translational flexure parallel mechanism were formulated in the design process. A parametric stiffness analysis of the Orthoglide was performed by Majou *et al.*[23] A compliant modeling and symbolic expressions of the stiffness matrix were formulated, which allowed a systematic analysis of the influence of the geometric design parameters and the identification of the critical link parameters. Chen and Lan[24] introduced a derivation and simulation technique for the instantaneous stiffness for the Stewart platform. The high nonlinearity of motions and driving forces of the parallel mechanisms were expressed and resulted in an asymmetric stiffness matrix. Other related stiffness modeling and kinematic analyses of different parallel manipulators can also be found.[25–36]

In this paper, the stiffness model of the Tri-pyramid Robot will be established based on the overall Jacobian matrix method. Li and Xu[37,38] analyzed stiffness models of two 3-DOF TPMs based on the overall Jacobian matrix method, while Wang *et al.*[39] presented a more detailed analytical approach for the stiffness modeling of the Tricept Robot by using the overall Jacobian matrix. The general formulation of the bending stiffness matrix of the passive links was considered in the compatibility conditions of the system. The overall Jacobian matrix includes the Jacobian of constraints and actuations for the limited-DOF parallel manipulators,[40] which was derived based on the theory of reciprocal screws.[41,42] In the stiffness modeling in this paper the overall Jacobian matrix, the stiffness of the fixed and moving platforms of the Tri-pyramid Robot will also be included by considering the stiffness of constraints (links) and actuations (actuators). Once the stiffness model is obtained, the stiffness performance will be evaluated by the extreme eigenvalues of the output stiffness matrix, because the output stiffness in an arbitrary direction is defined by the minimal and maximal eigenvalues of the stiffness matrix in a given pose.[17] Hence, the distribution of the output stiffness can be characterized by the distribution of the minimal and maximal eigenvalues in the manipulator's reachable workspace. By considering the variations of the structural parameters and the distribution of the output stiffness, the maximal stiffness workspace can be obtained through numerical optimization. This information provides the basic design constraints for the parameters of the Tri-pyramid Robot.

In the following Sections, the structural design of the Tri-pyramid Robot is, for the sake of completes, reviewed in Section 2 followed by the analysis of the inverse position solution of the closed-loop constraints in Section 3. The overall Jacobian matrix of constraints and actuations is built in Section 4. The stiffness of all components and the output stiffness matrix of the Tri-pyramid Robot are derived in Sections 5 and 6, respectively, followed by the evaluation of the workspace and stiffness distribution in Sections 7 and 8, respectively. The final conclusions are drawn in Section 9.

2. Structural Design

Usually, 3-DOF TPMs can be designed with three subchains connecting the moving platform to the fixed platform. Three actuators are respectively arranged in the three subchains to actuate the 3-DOF translational motions of the output moving platform. Based on displacement group theory,[43,44] a Schoenflies displacement subgroup (three orthogonal translations and a rotation) can be applied in each subchain of the 3-DOF TPM to constrain rotations and generate the common translations of

https://doi.org/10.1017/S0263574714001520 Published online by Cambridge University Press

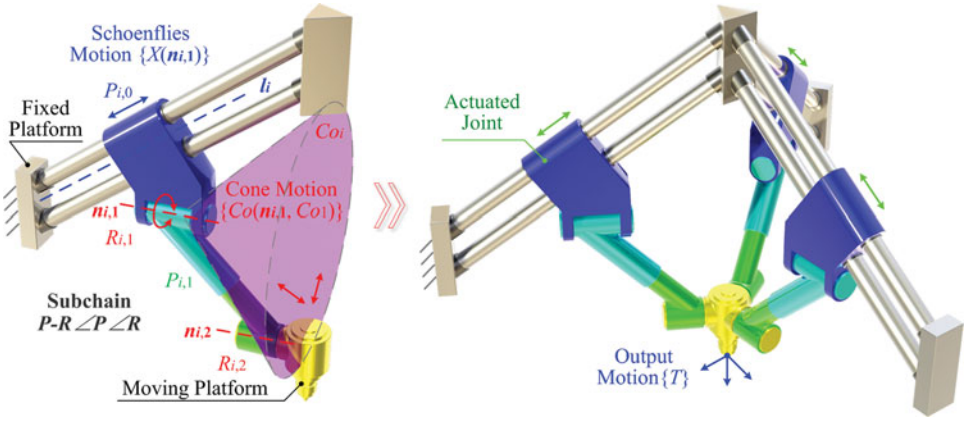


Fig. 1. Structural design of the Tri-pyramid Robot.

the output moving platform. The combination of a planar displacement subgroup and a translational displacement group is frequently used to build a Schoenflies displacement subgroup in the developed 3-DOF TPMs.[1–14] In the work of Kong *et al.*,[14] for example, the PRPR (P: prismatic joint, R: revolute joint) structure was listed. The parallelism of the two revolute joints was the only constraint specified. The other constraint relations between the joints in each subchain, and the connection relations between the three subchains were not given.

In this paper, in order to overcome the drawbacks of the developed 3-DOF TPMs, a conical displacement subset is defined and used to build the Schoenflies displacement subgroup in each subchain. The additional specified constraint relations between all the joints will be analyzed below.

As shown in Fig. 1, a conical displacement subset can be built by the serial joints $R_{i,1}P_{i,1}R_{i,2}$, where the prismatic joint $P_{i,1}$ connects the two parallel revolute joints $R_{i,1}$ and $R_{i,2}$ under an angle (the subscript i represents the i^{th} subchain). The serial joints $R_{i,1}P_{i,1}R_{i,2}$, namely, the conical displacement subset $\{Co(\boldsymbol{n_{i,1}}, Co_i)\}$ can generate a rotation $\{R(\boldsymbol{n_{i,1}})\}$ around the cone axis $\boldsymbol{n_{i,1}}$ and two translations $\{T(Co_i)\}$ on the cone surface Co_i, where the rotational axis of $\{R(\boldsymbol{n_{i,1}})\}$ can be determined as a moving direction as parallel with the $\boldsymbol{n_{i,1}}$. By combing a prismatic joint $P_{i,0}$ with the $R_{i,1}P_{i,1}R_{i,2}$ (the translational direction $\boldsymbol{l_i}$ of $P_{i,0}$ is arbitrarily related to the conical displacement subset), the structure for the Schoenflies motion $\{X(\boldsymbol{n_{i,1}})\}$ can be obtained as a subchain $P-R\angle P\angle R$. Three subchains $P-R\angle P\angle R$ can be combined in a symmetric form to build the 3-DOF TPM shown in Fig. 1 that will be referred to as the "Tri-pyramid Robot." In accordance with displacement group theory,[43,44] the intersection operation of the displacement subsets between the subchains is:

$$\begin{aligned} Z_m &= \bigcap_{i=1}^{3}\{X(\boldsymbol{n_{i,1}})\} = \bigcap_{i=1}^{3}[\{Co(\boldsymbol{n_{i,1}}, Co_i)\}\{T(\boldsymbol{l_i})\}] \\ &= \bigcap_{i=1}^{3}[\{R(\boldsymbol{n_{i,1}})\}\{T(Co_i)\}\{T(\boldsymbol{l_i})\}] \\ &= \bigcap_{i=1}^{3}[\{T(Co_i)\}\{T(\boldsymbol{l_i})\}] \\ &= \{T\} \end{aligned} \tag{1}$$

where the output motions Z_m of the moving platform are three orthogonal translations $\{T\}$. The actuated joint can be chosen as the prismatic joints $P_{i,0}$ of each subchain (the remaining joints $R_{i,1}P_{i,1}R_{i,2}$ are passive joints), because there are no intersection motions between the three conical displacement subsets in the different directions when the actuators of the three prismatic joints P_0 are locked. In order to avoid sticking of the passive prismatic joints, the three linear actuations will not be placed in a plane, and the intersection angle between the actuated prismatic joint and the passive prismatic joint in each subchain should not be 90°. It should also be noted that, in the reachable workspace, the intersection cure of any two cones of the subchains is not parallel with the moving direction of the passive prismatic joint of the third subchain. Thus, the output motion along the

https://doi.org/10.1017/S0263574714001520 Published online by Cambridge University Press

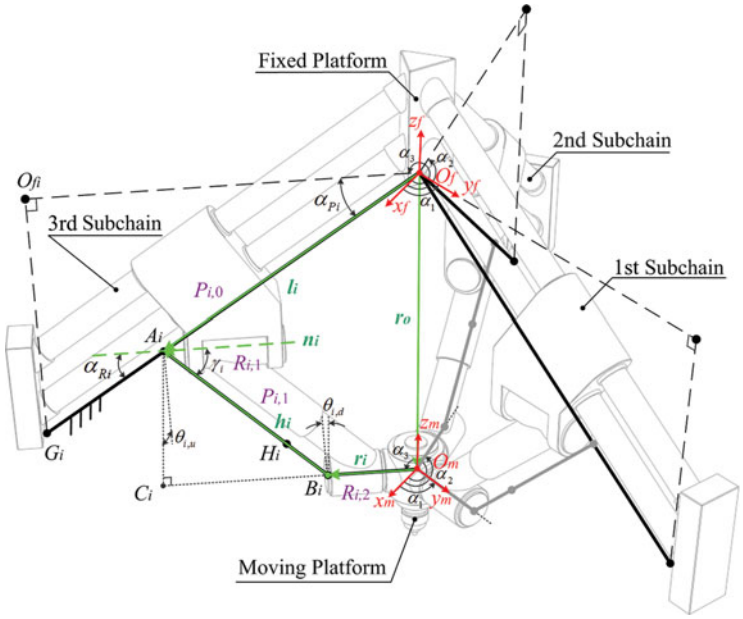


Fig. 2. Structural parameters of the Tri-pyramid Robot.

intersection cure can be actuated by the fixed prismatic joint of the third subchain. Three fixed input linear actuations can be designed in an orthogonal form. The three orthogonal output translations of the moving platform can be directly actuated by the three orthogonal linear actuations.

Compared to the developed 3-DOF TPMs,[1–14] the features of the Tri-pyramid Robot are:

(1) Three identical subchains are designed and arranged symmetrically in a non-Cartesian constraint configuration.
(2) Only four 1-DOF joints are included in each subchain, no universal or spherical joints are involved.
(3) The moving platform is connected with three revolute joints instead of universal or cylindrical joints. A relatively small size of the moving platform can be realized.
(4) All actuation is accomplished through linear actuators and placed on the fixed platform.

As a consequence of these features, a higher load/weight ratio and stiffness of the Tri-pyramid Robot can be expected in comparison to the developed 3-DOF TPMs.[1–14] The related kinematic position analysis, overall Jacobian, stiffness matrix determination, workspace, and stiffness evaluations are performed in the following sections.

3. Kinematic Position Solutions

In order to establish the stiffness model of the Tri-pyramid Robot, the kinematic position solutions should be determined to provide the constraint relations of the structure. The position relationships between the three linear input motions of actuations and the three translational output motions of the moving platform can be analyzed in a closed-loop form. In the following paragraphs the basic relations required for the stiffness analysis are reviewed.

In Fig. 2, a fixed reference frame $O_f - x_f y_f z_f$ is placed at the center of the fixed platform, and a parallel moving reference frame $O_m - x_m y_m z_m$ is defined at the center of the moving platform. The dashed lines $O_f O_{fi}$ (i =1, 2, 3) are projection lines of the guide ways $O_f G_i$ of the three linear actuators along the axis z_f in the plane $x_f O_f y_f$. The intersection angle between $O_f O_{fi}$ and $O_f G_i$ is α_{Pi}. The lines $O_f O_{fi}$ are arranged along the axis x_f with intersection angles α_1, α_2 and α_3, respectively. The prismatic joints and revolute joints $P_{i,0}$, $R_{i,1}$, $P_{i,1}$, and $R_{i,2}$ are connected in sequence. The basic structural parameters are α_i, α_{Pi}, α_{Ri}, γ_i, and $\|\boldsymbol{r_i}\|$, where α_{Ri} is the intersection angle between the axis of $R_{i,1}$ and the moving direction of $P_{i,0}$, γ_i represents the intersection angle between the axis of $R_{i,1}$ and the moving direction of $P_{i,1}$, while $\|\boldsymbol{r_i}\|$ is the size of the moving platform

https://doi.org/10.1017/S0263574714001520 Published online by Cambridge University Press

between points O_m and B_i which is parallel to the axis of $R_{i,1}$. The joint variables of $P_{i,0}$, $R_{i,1}$, $P_{i,1}$, and $R_{i,2}$ are $\|\boldsymbol{l_i}\|$, $\theta_{i,u}$, $\|\boldsymbol{h_i}\|$, and $\theta_{i,d}$, respectively. The input variables are the lengths of travel $\|\boldsymbol{l_i}\|$ of the linear actuators between points O_f and A_i which is along the three guide ways, while the output variable is the position vector $\boldsymbol{r_O}$ (x, y, z) of the moving platform between points O_f and O_m. In a subchain, the kinematic constraint of the closed loop is:

$$\boldsymbol{l_i} = \boldsymbol{r_O} + \boldsymbol{r_i} + \boldsymbol{h_i} \tag{2}$$

where the constituent vectors are defined as:

$$\begin{cases} \boldsymbol{l_i} = \overrightarrow{O_f A_i} = [\|\boldsymbol{l_i}\| \cos\alpha_{Pi} \cos\alpha_i \quad \|\boldsymbol{l_i}\| \cos\alpha_{Pi} \sin\alpha_i \quad \|\boldsymbol{l_i}\| \sin\alpha_{Pi}]^T \\ \boldsymbol{r_O} = \overrightarrow{O_f O_m} = [x \quad y \quad z]^T \\ \boldsymbol{r_i} = \overrightarrow{O_m B_i} = \overrightarrow{O_f B_i} - \overrightarrow{O_f O_m} \\ \quad = [\|\boldsymbol{r_i}\| \cos(\alpha_{Pi} - \alpha_{Ri}) \cos\alpha_i \quad \|\boldsymbol{r_i}\| \cos(\alpha_{Pi} - \alpha_{Ri}) \sin\alpha_i \quad \|\boldsymbol{r_i}\| \sin(\alpha_{Pi} - \alpha_{Ri})]^T \\ \quad = \boldsymbol{n_i} \end{cases} \tag{3}$$

Thus, the vector $\mathbf{h_i}$ can be deduced as:

$$\boldsymbol{h_i} = \overrightarrow{B_i A_i} = \boldsymbol{l_i} - \boldsymbol{r_i} - \boldsymbol{r_O} \quad = \begin{bmatrix} (\|\boldsymbol{l_i}\| \cos\alpha_{Pi} - \|\boldsymbol{r_i}\| \cos(\alpha_{Pi} - \alpha_{Ri})) \cos\alpha_i - x \\ (\|\boldsymbol{l_i}\| \cos\alpha_{Pi} - \|\boldsymbol{r_i}\| \cos(\alpha_{Pi} - \alpha_{Ri})) \sin\alpha_i - y \\ \|\boldsymbol{l_i}\| \sin\alpha_{Pi} - \|\boldsymbol{r_i}\| \sin(\alpha_{Pi} - \alpha_{Ri}) - z \end{bmatrix} \tag{4}$$

In accordance with the structural constraint condition, namely, the intersection angle between variable vectors $\boldsymbol{n_i}$ and $\boldsymbol{h_i}$ is constant γ_i, the corresponding kinematic constraint equation can be obtained by the dot product of $\boldsymbol{n_i}$ and $\boldsymbol{h_i}$ as:

$$\begin{aligned} \boldsymbol{n_i} \cdot \boldsymbol{h_i} &= \|\boldsymbol{r_i}\| \cos(\alpha_{Pi} - \alpha_{Ri}) \cos\alpha_i \left((\|\boldsymbol{l_i}\| \cos\alpha_{Pi} - \|\boldsymbol{r_i}\| \cos(\alpha_{Pi} - \alpha_{Ri})) \cos\alpha_i - x\right) \\ &\quad + \|\boldsymbol{r_i}\| \cos(\alpha_{Pi} - \alpha_{Ri}) \sin\alpha_i \left((\|\boldsymbol{l_i}\| \cos\alpha_{Pi} - \|\boldsymbol{r_i}\| \cos(\alpha_{Pi} - \alpha_{Ri})) \sin\alpha_i - y\right) \\ &\quad + \|\boldsymbol{r_i}\| \sin(\alpha_{Pi} - \alpha_{Ri}) \left(\|\boldsymbol{l_i}\| \sin\alpha_{Pi} - \|\boldsymbol{r_i}\| \sin(\alpha_{Pi} - \alpha_{Ri}) - z\right) \\ &= \|\boldsymbol{n_i}\| \, \|\boldsymbol{h_i}\| \cos\gamma_i \\ &= \|\boldsymbol{r_i}\| \cos\gamma_i \sqrt{\begin{array}{l} ((\|\boldsymbol{l_i}\| \cos\alpha_{Pi} - \|\boldsymbol{r_i}\| \cos(\alpha_{Pi} - \alpha_{Ri})) \cos\alpha_i - x)^2 \\ \quad + ((\|\boldsymbol{l_i}\| \cos\alpha_{Pi} - \|\boldsymbol{r_i}\| \cos(\alpha_{Pi} - \alpha_{Ri})) \sin\alpha_i - y)^2 \\ \quad + (\|\boldsymbol{l_i}\| \sin\alpha_{Pi} - \|\boldsymbol{r_i}\| \sin(\alpha_{Pi} - \alpha_{Ri}) - z)^2 \end{array}} \end{aligned} \tag{5}$$

To solve Eq. (5) with respect to the unknown parameter $\|\boldsymbol{l_i}\|$, the inverse kinematic position solution of the Tri-pyramid Robot can be obtained as:

$$\|\boldsymbol{l_i}\| = \frac{\|\boldsymbol{r_i}\| \cos\alpha_{Ri} \sin^2\gamma_i + E_{Bi} \cos\alpha_{Ri} - E_{Ai} \cos^2\gamma_i \pm \sqrt{\begin{array}{l} \left(\|\boldsymbol{r_i}\| \cos\alpha_{Ri} \sin^2\gamma_i + E_{Bi} \cos\alpha_{Ri} - E_{Ai} \cos^2\gamma_i\right)^2 - \\ \left(\cos^2\alpha_{Ri} - \cos^2\gamma_i\right) \\ \left((\|\boldsymbol{r_i}\| + E_{Bi})^2 - \cos^2\gamma_i \left(\|\boldsymbol{r_i}\|^2 + x^2 + y^2 + z^2 + 2\|\boldsymbol{r_i}\| E_{Bi}\right)\right) \end{array}}}{\cos^2\alpha_{Ri} - \cos^2\gamma_i} \tag{6}$$

where E_{Ai} and E_{Bi} are:

$$\begin{cases} E_{Ai} = x \cos\alpha_{Pi} \cos\alpha_i + y \cos\alpha_{Pi} \sin\alpha_i + z \sin\alpha_{Pi} \\ E_{Bi} = x \cos(\alpha_{Pi} - \alpha_{Ri}) \cos\alpha_i + y \cos(\alpha_{Pi} - \alpha_{Ri}) \sin\alpha_i + z \sin(\alpha_{Pi} - \alpha_{Ri}) \end{cases} \tag{7}$$

https://doi.org/10.1017/S0263574714001520 Published online by Cambridge University Press

In Eq. (6), the symbol "±" is set to "+" for the larger value because the $\|\boldsymbol{l_i}\|$ is a non-negative number, and the initial positions of the slide blocks are placed outward from the symmetric center point O_m.

Correspondingly, the forward kinematic position solution can be obtained by solving Eq. (6) for the unknown output variables x, y, and z when the input variables $\|\boldsymbol{l_i}\|$ are given. Based on the kinematic position solutions, the overall Jacobian matrix will be developed in the next section for stiffness modeling.

4. Overall Jacobian Matrix

In order to establish the stiffness model of the Tri-pyramid Robot, all of the deformations including three rotations and three translations of the moving platform should be considered. Thus, a 6×6 overall Jacobian matrix is required for the stiffness modeling of this limited-DOF parallel manipulator. The overall Jacobian matrix includes the Jacobian of the constraints and actuations.[40] Correspondingly, the stiffness of structural constraints and the stiffness of actuations can be included in the 6×6 overall Jacobian matrix, respectively. Based on the theory of reciprocal screws,[41,42] the Jacobian of constraints and actuations are analyzed as follows.

By assuming that the deformations of the output moving platform include 6-DOF motions, the vectors for the angular and linear velocities of the moving platform can be respectively expressed in the fixed reference frame $O_f - x_f y_f z_f$ as:

$$\begin{cases} \boldsymbol{\omega} = [\omega_{xf} \quad \omega_{yf} \quad \omega_{zf}]^T \\ \boldsymbol{v} = [v_{xf} \quad v_{yf} \quad v_{zf}]^T \end{cases} \tag{8}$$

Based on the closed-loop constraint of each subchain in Eq. (2), the instantaneous twist $\$_{\boldsymbol{Om}}$ of the moving platform is a linear combination of the four instantaneous twists of the joints, namely:

$$\$_{\boldsymbol{Om}} = [\boldsymbol{\omega}^T \quad \boldsymbol{v}^T]^T = \|\dot{\boldsymbol{l}}_{\boldsymbol{i}}\| \hat{\$}_{\boldsymbol{i,1}} + \theta^{\bullet}_{i,u} \hat{\$}_{\boldsymbol{i,2}} + \|\dot{\boldsymbol{h}}_{\boldsymbol{i}}\| \$'^{U}_{\boldsymbol{i,3}} + \theta^{\bullet}_{i,d} \hat{\$}_{\boldsymbol{i,4}} \tag{9}$$

where $\hat{\$}_{\boldsymbol{i,j}}$ (i =1, 2, and 3, j = 1, 2, 3, and 4) is a unit screw associated with the j^{th} joint of the i^{th} subchain. $\|\boldsymbol{l_i}\|^{\bullet}$, $\theta^{\bullet}_{i,u}$, $\|\boldsymbol{h_i}\|^{\bullet}$, and $\theta^{\bullet}_{i,d}$, represent the velocities of the joints. The linear combination of the instantaneous twists of each subchain is the same because the three subchains are connected to the moving platform and constrained with identical output motions.

In Fig. 3, the unit vector $\boldsymbol{s_{i,j}}$ that is along the j^{th} joint axis of the i^{th} subchain is given by:

$$\boldsymbol{s_{i,1}} = \frac{\boldsymbol{l_i}}{\|\boldsymbol{l_i}\|} = [\cos\alpha_{Pi}\cos\alpha_i \quad \cos\alpha_{Pi}\sin\alpha_i \quad \sin\alpha_{Pi}]^T \tag{10}$$

$$\boldsymbol{s_{i,2}} = \boldsymbol{s_{i,4}} = \frac{\boldsymbol{r_i}}{\|\boldsymbol{r_i}\|} = \left[\cos(\alpha_{Pi} - \alpha_{Ri})\cos\alpha_i \quad \cos(\alpha_{Pi} - \alpha_{Ri})\sin\alpha_i \quad \sin(\alpha_{Pi} - \alpha_{Ri})\right]^T \tag{11}$$

$$\boldsymbol{s_{i,3}} = \frac{\boldsymbol{h_i}}{\|\boldsymbol{h_i}\|} = \frac{\begin{bmatrix} (\|\boldsymbol{l_i}\|\cos\alpha_{Pi} - \|\boldsymbol{r_i}\|\cos(\alpha_{Pi} - \alpha_{Ri}))\cos\alpha_i - x \\ (\|\boldsymbol{l_i}\|\cos\alpha_{Pi} - \|\boldsymbol{r_i}\|\cos(\alpha_{Pi} - \alpha_{Ri}))\sin\alpha_i - y \\ \|\boldsymbol{l_i}\|\sin\alpha_{Pi} - \|\boldsymbol{r_i}\|\sin(\alpha_{Pi} - \alpha_{Ri}) - z \end{bmatrix}}{\sqrt{\begin{array}{c} ((\|\boldsymbol{l_i}\|\cos\alpha_{Pi} - \|\boldsymbol{r_i}\|\cos(\alpha_{Pi} - \alpha_{Ri}))\cos\alpha_i - x)^2 \\ + ((\|\boldsymbol{l_i}\|\cos\alpha_{Pi} - \|\boldsymbol{r_i}\|\cos(\alpha_{Pi} - \alpha_{Ri}))\sin\alpha_i - y)^2 \\ + (\|\boldsymbol{l_i}\|\sin\alpha_{Pi} - \|\boldsymbol{r_i}\|\sin(\alpha_{Pi} - \alpha_{Ri}) - z)^2 \end{array}}} \tag{12}$$

where $\|\boldsymbol{l_i}\|$ can be obtained from Eq. (6). Thus, the unit screws $\hat{\$}_{\boldsymbol{i,j}}$ of Eq. (9) are:

$$\hat{\$}_{\boldsymbol{i,1}} = \begin{bmatrix} \boldsymbol{0} \\ \boldsymbol{s_{i,1}} \end{bmatrix} \tag{13}$$

https://doi.org/10.1017/S0263574714001520 Published online by Cambridge University Press

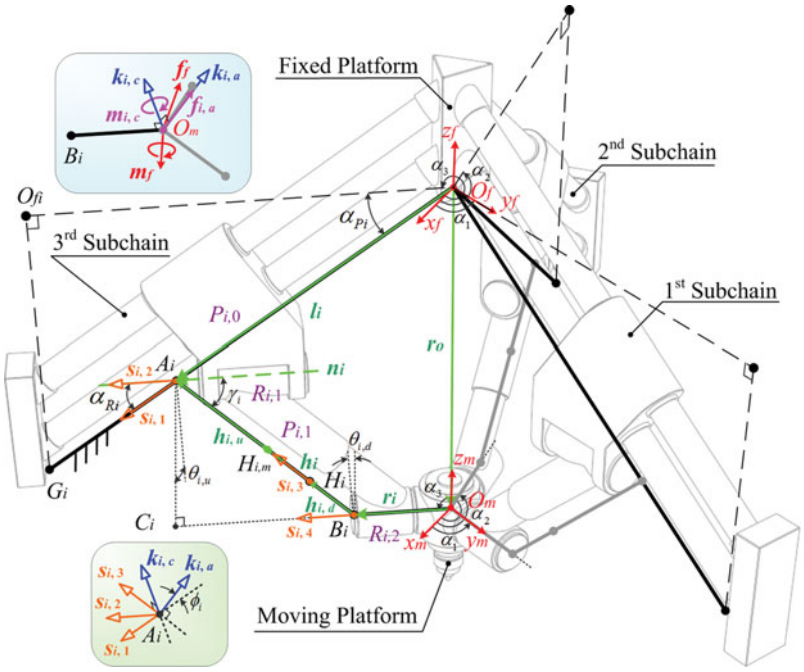


Fig. 3. Screws and loads of the Tri-pyramid Robot.

$$\hat{\$}_{i,2} = \begin{bmatrix} \boldsymbol{s}_{i,2} \\ \overrightarrow{O_m A_i} \times \boldsymbol{s}_{i,2} \end{bmatrix} = \begin{bmatrix} \boldsymbol{s}_{i,2} \\ (\boldsymbol{r}_i + \boldsymbol{h}_i) \times \boldsymbol{s}_{i,2} \end{bmatrix} \tag{14}$$

$$\hat{\$}_{i,3} = \begin{bmatrix} \boldsymbol{0} \\ \boldsymbol{s}_{i,3} \end{bmatrix} \tag{15}$$

$$\hat{\$}_{i,4} = \begin{bmatrix} \boldsymbol{s}_{i,4} \\ \boldsymbol{0} \times \boldsymbol{s}_{i,4} \end{bmatrix} \tag{16}$$

In accordance with the theory of reciprocal screws,[41,42] a reciprocal screw $\$_a \circ \$_b$ is that the wrench $\$_a$ has no work along the twist of $\$_b$. In each subchain of the Tri-pyramid Robot, a unit constraint screw $\hat{\$}_{i,c}$ is reciprocal to all joint screws (instantaneous twist $\$_{Om}$ of the moving platform). The wrench $\hat{\$}_{i,c}$ cannot activate the motions of the four joints of each subchain. Thus, based on the structural constraints of the joints in each subchain, the unit constraint screw $\hat{\$}_{i,c}$ can be identified as an infinite-pitch wrench screw, namely:

$$\hat{\$}_{i,c} = \begin{bmatrix} \boldsymbol{0} \\ \boldsymbol{k}_{i,c} \end{bmatrix} = \begin{bmatrix} \boldsymbol{0} \\ \frac{\boldsymbol{s}_{i,2} \times \boldsymbol{s}_{i,3}}{\|\boldsymbol{s}_{i,2} \times \boldsymbol{s}_{i,3}\|} \end{bmatrix} = \begin{bmatrix} \boldsymbol{0} \\ \frac{\boldsymbol{s}_{i,2} \times \boldsymbol{s}_{i,3}}{|\sin \gamma_i|} \end{bmatrix} \tag{17}$$

which represents a unit couple of constraints imposed by the joints of the i^{th} subchain, and the couple is exerted on the moving platform around the direction of the unit constraint vector $\boldsymbol{k}_{i,c}$. The constraint vector $\boldsymbol{k}_{i,c}$, is perpendicular to the unit vectors $\boldsymbol{s}_{i,2}$ and $\boldsymbol{s}_{i,3}$. The reciprocal product of the unit constraint screw $\hat{\$}_{i,c}$ and of the instantaneous twist $\$_{Om}$ is:

$$\hat{\$}_{i,c} \circ \$_{Om} = \left(\nabla \hat{\$}_{i,c}\right)^T \$_{Om} = \boldsymbol{J}_{i,c} \$_{Om} = 0 \tag{18}$$

https://doi.org/10.1017/S0263574714001520 Published online by Cambridge University Press

where the transformation matrix ∇ is:

$$\nabla = \begin{bmatrix} 0 & 0 & 0 & 1 & 0 & 0 \\ 0 & 0 & 0 & 0 & 1 & 0 \\ 0 & 0 & 0 & 0 & 0 & 1 \\ 1 & 0 & 0 & 0 & 0 & 0 \\ 0 & 1 & 0 & 0 & 0 & 0 \\ 0 & 0 & 1 & 0 & 0 & 0 \end{bmatrix} \tag{19}$$

Thus, the Jacobian of constraints can be obtained from Eq. (18), which transforms the angular and linear velocities of the moving platform to 0. By considering the constraints of the three subchains, the Jacobian of the constraints is:

$$\boldsymbol{J_c} = \begin{bmatrix} \boldsymbol{J_{1,c}} \\ \boldsymbol{J_{2,c}} \\ \boldsymbol{J_{3,c}} \end{bmatrix} = \begin{bmatrix} \boldsymbol{k_{1,c}^T} & 0 & 0 & 0 \\ \boldsymbol{k_{2,c}^T} & 0 & 0 & 0 \\ \boldsymbol{k_{3,c}^T} & 0 & 0 & 0 \end{bmatrix} \tag{20}$$

where $\boldsymbol{k_{i,c}}$ is determined in Eq. (17). Each row of $\boldsymbol{J_c}$ represents a unit wrench of structural constraints of a subchain, which is exerted on the moving platform. Thus, the Jacobian of constraints determines the 3-DOF translational output motions of the moving platform.

If $\boldsymbol{J_c}$ is of full rank, the unique solution for $\boldsymbol{J_{i,c}\$_{Om}} = 0$ (Eq. (18)) is $\boldsymbol{\omega} = 0$. Thus, based on Eqs. (9) and (13)–(16), a constraint equation can be obtained as:

$$\dot{\theta}_{i,u}\, \boldsymbol{s_{i,2}} + \dot{\theta}_{i,d}\, \boldsymbol{s_{i,4}} = 0 \tag{21}$$

Since $\boldsymbol{s_{i,2}} = \boldsymbol{s_{i,4}} \neq 0$, thus, Eq. (21) can be deduced as:

$$\dot{\theta}_{i,u} + \dot{\theta}_{i,d} = 0 \tag{22}$$

stating that the magnitudes of the rotational angles of joints $R_{i,1}$ and $R_{i,2}$ are equal.

By assuming that the actuated joint ($P_{i,0}$) in each subchain is locked, a unit actuation screw $\hat{\$}_{\boldsymbol{i,a}}$ is reciprocal to all passive joint ($R_{i,1}P_{i,1}R_{i,2}$) screws of the i^{th} subchain. The wrench of $\hat{\$}_{\boldsymbol{i,a}}$ has no work on all passive joints but the actuated joint. Thus, the unit actuation screw $\hat{\$}_{\boldsymbol{i,a}}$ can be identified as a zero-pitch screw along the direction of the unit actuation vector $\boldsymbol{k_{i,a}}$, i.e.:

$$\hat{\$}_{\boldsymbol{i,a}} = \begin{bmatrix} \boldsymbol{k_{i,a}} \\ \boldsymbol{r_i} \times \boldsymbol{k_{i,a}} \end{bmatrix} = \begin{bmatrix} \frac{\boldsymbol{k_{i,c}} \times \boldsymbol{s_{i,3}}}{\|\boldsymbol{k_{i,c}} \times \boldsymbol{s_{i,3}}\|} \\ \mathbf{r_i} \times \left(\frac{\boldsymbol{k_{i,c}} \times \boldsymbol{s_{i,3}}}{\|\boldsymbol{k_{i,c}} \times \boldsymbol{s_{i,3}}\|} \right) \end{bmatrix} = \begin{bmatrix} \boldsymbol{k_{i,c}} \times \boldsymbol{s_{i,3}} \\ \boldsymbol{r_i} \times \left(\boldsymbol{k_{i,c}} \times \boldsymbol{s_{i,3}} \right) \end{bmatrix} \tag{23}$$

which represents a unit force of actuation imposed by the actuated joint of the i^{th} subchain that is exerted on the moving platform along the direction of the unit actuation vector $\boldsymbol{k_{i,a}}$. The vector $\boldsymbol{k_{i,a}}$ is perpendicular to the unit vectors $\boldsymbol{s_{i,3}}$ and passes through the axes of joints $R_{i,1}$ and $R_{i,2}$. The reciprocal product of the unit actuation screw $\hat{\$}_{\boldsymbol{i,a}}$ and of the instantaneous twist $\boldsymbol{\$_{Om}}$ is:

$$\hat{\$}_{\boldsymbol{i,a}} \circ \boldsymbol{\$_{Om}} = \left(\nabla\, \hat{\$}_{\boldsymbol{i,a}} \right)^T \boldsymbol{\$_{Om}} = \|\dot{\boldsymbol{l}}_{\boldsymbol{i}}\| \cos\phi_i = \|\dot{\boldsymbol{l}}_{\boldsymbol{i}}\|\, \boldsymbol{k_{i,a}^T s_{i,1}} \tag{24}$$

where ϕ_i is intersection angle between $\boldsymbol{k_{i,a}}$ and $\boldsymbol{s_{i,1}}$. Equation (24) can be transformed as:

$$\boldsymbol{J_{i,a}\$_{Om}} = \begin{bmatrix} \frac{(\boldsymbol{r_i} \times \boldsymbol{k_{i,a}})^T}{\boldsymbol{k_{i,a}^T s_{i,1}}} & \frac{\boldsymbol{k_{i,a}^T}}{\boldsymbol{k_{i,a}^T s_{i,1}}} \end{bmatrix} \boldsymbol{\$_{Om}} = \|\dot{\boldsymbol{l}}_{\boldsymbol{i}}\| \tag{25}$$

Thus, the Jacobian of actuations is determined by Eq. (25), which transforms the angular and linear velocities of the moving platform to the linear input velocity $\|\dot{\boldsymbol{l}}_{\boldsymbol{i}}\|$ of the actuator. By considering the

https://doi.org/10.1017/S0263574714001520 Published online by Cambridge University Press

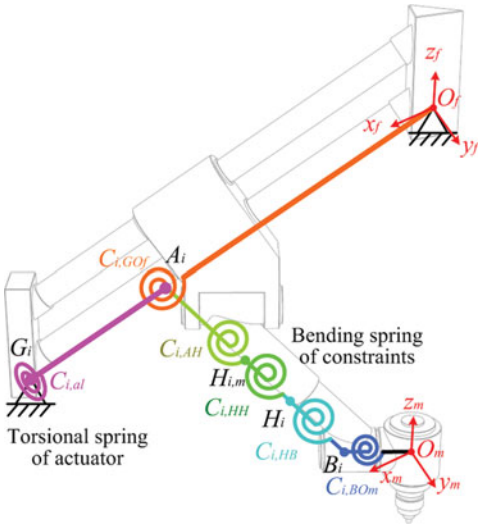


Fig. 4. Equivalent spring structure of a subchain.

motions of the three subchains, the Jacobian of actuations assumes the form:

$$\boldsymbol{J}_a = \begin{bmatrix} \boldsymbol{J}_{1,a} \\ \boldsymbol{J}_{2,a} \\ \boldsymbol{J}_{3,a} \end{bmatrix} = \begin{bmatrix} \frac{(\boldsymbol{r}_1 \times \boldsymbol{k}_{1,a})^T}{\boldsymbol{k}_{1,a}^T \boldsymbol{s}_{1,1}} & \frac{\boldsymbol{k}_{1,a}^T}{\boldsymbol{k}_{1,a}^T \boldsymbol{s}_{1,1}} \\ \frac{(\boldsymbol{r}_2 \times \boldsymbol{k}_{2,a})^T}{\boldsymbol{k}_{2,a}^T \boldsymbol{s}_{2,1}} & \frac{\boldsymbol{k}_{2,a}^T}{\boldsymbol{k}_{2,a}^T \boldsymbol{s}_{2,1}} \\ \frac{(\boldsymbol{r}_3 \times \boldsymbol{k}_{3,a})^T}{\boldsymbol{k}_{3,a}^T \boldsymbol{s}_{3,1}} & \frac{\boldsymbol{k}_{3,a}^T}{\boldsymbol{k}_{3,a}^T \boldsymbol{s}_{3,1}} \end{bmatrix} \tag{26}$$

In accordance with the Jacobian of constraints and actuations, the overall velocity transformation from the output moving platform to the input actuated joint of each subchain is:

$$\boldsymbol{J}_i \$_{Om} = \begin{bmatrix} \boldsymbol{J}_{i,a} \\ \boldsymbol{J}_{i,c} \end{bmatrix} \$_{Om} = \begin{bmatrix} \|\dot{\boldsymbol{l}}_i\| \\ 0 \end{bmatrix} \tag{27}$$

Thus, the 6×6 overall Jacobian matrix of the Tri-pyramid Robot is given by:

$$\boldsymbol{J} = \begin{bmatrix} \boldsymbol{J}_a \\ \boldsymbol{J}_c \end{bmatrix} = \begin{bmatrix} \boldsymbol{J}_{1,a} & \boldsymbol{J}_{2,a} & \boldsymbol{J}_{3,a} & \boldsymbol{J}_{1,c} & \boldsymbol{J}_{2,c} & \boldsymbol{J}_{3,c} \end{bmatrix}^T \tag{28}$$

which is a 6×6 transformation matrix including all of the basic constraints and actuations of transformation between all joints motions and output motions of the moving platform.

5. Stiffness Analysis of a Subchain

In the structure of the Tri-pyramid Robot, the stiffness of all links, joints, actuators, fixed, and moving platforms are included in the stiffness model. In accordance with the analysis of the overall Jacobian matrix, in each subchain the actuation screw $\hat{\$}_{i,a}$ imposes an actuation force $\boldsymbol{f}_{i,a}$ at point C_i of the moving platform along the directions of $\boldsymbol{k}_{i.a}$, while the constraint screw $\hat{\$}_{i,c}$ exerts a constraint couple $\boldsymbol{M}_{i,c}$ at point C_i of the moving platform around the direction of $\boldsymbol{k}_{i.c}$ as shown in Fig. 3. Thus, the overall deformations of each subchain are simultaneously generated by the actuation force $\boldsymbol{f}_{i,a}$ and the constraint couple $\boldsymbol{M}_{i,c}$.

In Fig. 4, the stiffness of a subchain can be considered as consisting of a serial connection of springs representing the stiffness of all links. Thus, by considering the effects of the actuation force and of the constraint couple, the following four components of the equivalent springs of a subchain can be identified:

https://doi.org/10.1017/S0263574714001520 Published online by Cambridge University Press

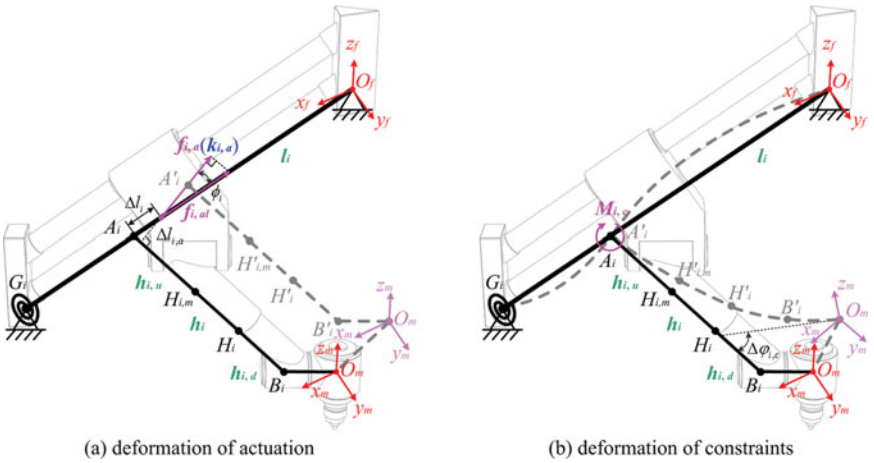


Fig. 5. Deformations of a subchain.

(1) If a lead screw is used, a torsional spring can be used to represent the stiffness of actuation. The rotational deformation of the actuator can be transformed as a linear deformation along the guide way. The compliance of the torsional spring is denoted by $C_{i,al}$. Equivalently, if a linear motor is used for actuation, a tensional spring is used to represent the stiffness of actuation. The linear deformation is along the guide way without a displacement transformation between the rotation and translation.
(2) In the guide way $O_f G_i$, a bending spring is used to represent the stiffness of the part of the fixed platform. The corresponding compliance is $C_{i,GOf}$.
(3) In the prismatic joint $P_{i,1}$, the guide way and the slide block have different bending stiffnesses. Thus, the equivalent spring between the points A_i and B_i can be separated into three parts, namely, guide way $A_i H_{i,m}$, slide block $H_i B_i$, and $H_{i,m} H_i$ (overlapping part between the guide way and the slide block). The compliances of $A_i H_{i,m}$, $H_i B_i$, and $H_{i,m} H_i$ are denoted as $C_{i,AH}$, $C_{i,HB}$, and $C_{i,HH}$, respectively.
(4) In the link $B_i O_m$, a bending spring is used to represent the stiffness of the part of the moving platform. The compliance of the link is denoted as $C_{i,BOm}$.

Tensional and compressional stiffnesses (along the direction of vector $\boldsymbol{h_i}$) do not exist in the prismatic joint $P_{i,1}$ because $P_{i,1}$ is a passive joint, and the actuation force $\boldsymbol{f_{i,a}}$ is perpendicular to the vector $\boldsymbol{h_i}$. Similarly, there is no torsional compliance around the vector $\boldsymbol{h_i}$ since the direction of the constraint couple $\boldsymbol{M_{i,c}}$ is perpendicular to the vector $\boldsymbol{h_i}$. Thus, in a subchain, there is a total of one torsional spring and five bending springs that can be used to represent the equivalent spring structure. In the static balance of the equivalent spring structure, the deformations of a subchain include both the deformations of actuation and of the constraints as shown in Fig. 5. The compliance of each spring can be deduced as follows.

In the case of lead screw in the i^{th} subchain, the torque $\tau_{i,a}$ of the actuator can be expressed as:

$$\tau_{i,a} = K_{i,\alpha a} \Delta\alpha_{i,a} \tag{29}$$

where $K_{i,\alpha a}$ and $\Delta\alpha_{i,a}$ represent the torsional stiffness and angular deformation of the actuator. By considering the torque transmission of the lead screw, the actuation force $\boldsymbol{f_{i,al}}$ is acting on the slide block and along the guide way $O_f G_i$, which can be deduced as:

$$\left\| \boldsymbol{f_{i,al}} \right\| = \frac{2\tau_{i,a}}{d_{i,a} \tan\left(\lambda_{i,a} + \psi_{i,a}\right)} \tag{30}$$

$$\begin{cases} \lambda_{i,a} = \tan^{-1}\left(\frac{L_{i,a}}{\pi d_{i,a}}\right) \\ \psi_{i,a} = \tan^{-1}\left(\frac{\mu_{i,c}}{\cos\alpha_{i,t}}\right) \end{cases} \tag{31}$$

https://doi.org/10.1017/S0263574714001520 Published online by Cambridge University Press

where $d_{i,a}$ and $L_{i,a}$ represent the pitch diameter and lead of the lead screw respectively. $\lambda_{i,a}$ and $\psi_{i,a}$ are the lead angle and the friction angle of the lead screw respectively, while $\alpha_{i,t}$ and $\mu_{i,c}$ are the radial angle of the thread and the coefficient of friction between the screw and nut. In Fig. 5(a), the linear displacement of the slide block is:

$$\Delta l_i = L_{i,a} \Delta \alpha_{i,a} \tag{32}$$

which is induced by the angular deformation of the actuator. Thus, the compliance of the torsional spring of the actuation can be deduced from Eqs. (29)–(32) as:

$$C_{i,al} = \frac{\Delta l_i}{\left\| \boldsymbol{f}_{\boldsymbol{i,al}} \right\|} = \frac{L_{i,a} d_{i,a} \tan\left(\lambda_{i,a} + \psi_{i,a}\right)}{2K_{i,\alpha a}} \tag{33}$$

In Fig. 5(b), based on the deformation of the constraints, the bending compliance of the guide way $O_f G_i$ is:

$$C_{i,GOf} = \frac{\Delta \varphi_{i,GOf}}{\left\| \boldsymbol{M}_{\boldsymbol{i,c}} \right\|} = \frac{(\|\boldsymbol{l_i}\|_{\max} - \|\boldsymbol{l_i}\|_{\min})^2 - 3\,(\|\boldsymbol{l_i}\| - \|\boldsymbol{l_i}\|_{\min})^2 - 3\,(\|\boldsymbol{l_i}\|_{\max} - \|\boldsymbol{l_i}\|)^2}{6EI_{ik,GOf}\,(\|\boldsymbol{l_i}\|_{\max} - \|\boldsymbol{l_i}\|_{\min})} \tag{34}$$

where $\Delta \varphi_{i,GOf}$ is the angular deformation of the guide way $O_f G_i$, $\|\boldsymbol{l_i}\|_{\min}$, and $\|\boldsymbol{l_i}\|_{\max}$ represent the moving range of the slide block, E is Young's modulus of elasticity, and $I_{ik,GOf}$ is the cross section moment of inertia of guide way $O_f G_i$ around the direction $\boldsymbol{k_{i.c}}$.

In the joint $P_{i,1}$, the bending compliances of $A_i H_{i,m}$, $H_{i,m} H_i$, and $H_i B_i$ can be respectively determined as:

$$C_{i,AH} = \frac{\Delta \varphi_{i,AH}}{\left\| \boldsymbol{M}_{\boldsymbol{i,c}} \right\|} = \frac{\|\boldsymbol{h_i}\| - \overrightarrow{H_{i,m} B_i}}{EI_{ik,AH}} = \frac{\|\boldsymbol{h_i}\| - \left\| \boldsymbol{h}_{\boldsymbol{i,d}} \right\|}{EI_{ik,AH}} \tag{35}$$

$$C_{i,HH} = \frac{\Delta \varphi_{i,HH}}{\left\| \boldsymbol{M}_{\boldsymbol{i,c}} \right\|} = \frac{\|\boldsymbol{h_i}\| - \overrightarrow{H_{i,m} B_i} - \overrightarrow{A_i H_i}}{EI_{ik,HH}} = \frac{\left\| \boldsymbol{h}_{\boldsymbol{i,d}} \right\| + \left\| \boldsymbol{h}_{\boldsymbol{i,u}} \right\| - \|\boldsymbol{h_i}\|}{EI_{ik,HH}} \tag{36}$$

$$C_{i,HB} = \frac{\Delta \varphi_{i,HB}}{\left\| \boldsymbol{M}_{\boldsymbol{i,c}} \right\|} = \frac{\|\boldsymbol{h_i}\| - \overrightarrow{A_i H_i}}{EI_{ik,HB}} = \frac{\|\boldsymbol{h_i}\| - \left\| \boldsymbol{h}_{\boldsymbol{i,u}} \right\|}{EI_{ik,HB}} \tag{37}$$

The bending compliance of link $B_i O_m$ is:

$$C_{i,BOm} = \frac{\Delta \varphi_{i,BOm}}{\left\| \boldsymbol{M}_{\boldsymbol{i,c}} \right\|} = \frac{\|\boldsymbol{r_i}\|}{EI_{ik,BOm}} \tag{38}$$

Thus, in the serial connection of the springs, the equivalent stiffness of a subchain can be respectively determined as the stiffness of the actuation and constraints as:

$$K_{i,al} = C_{i,al}^{-1} = \frac{\left\| \boldsymbol{f}_{\boldsymbol{i,al}} \right\|}{\Delta l_i} = \frac{2K_{i,\alpha a}}{L_{i,a} d_{i,a} \tan\left(\lambda_{i,a} + \psi_{i,a}\right)} \tag{39}$$

$$K_{i,c} = C_{i,c}^{-1} = \frac{\left\| \boldsymbol{M}_{\boldsymbol{i,c}} \right\|}{\Delta \varphi_{i,c}} = \left(C_{i,GOf} + C_{i,AH} + C_{i,HH} + C_{i,HB} + C_{i,BOm}\right)^{-1} \tag{40}$$

By combing the equivalent stiffnesses of the three subchains in the closed-loop form, the overall stiffness of the Tri-pyramid Robot can be obtained and analyzed. This will be presented in the next section.

https://doi.org/10.1017/S0263574714001520 Published online by Cambridge University Press

6. Stiffness Matrix Determination of the Tri-pyramid Robot

In order to establish the stiffness model of the Tri-pyramid Robot, the overall stiffness of the three subchains can be analyzed by the load/displacement ratio of the moving platform. By assuming that there are no preloads and gravity effects on the structure, the output force and torque exerted on the moving platform are:

$$\begin{cases} \boldsymbol{f}_f = [f_{xf} \quad f_{yf} \quad f_{zf}]^T \\ \boldsymbol{M}_f = [M_{xf} \quad M_{yf} \quad M_{zf}]^T \end{cases} \tag{41}$$

which can be expressed as an output wrench $\boldsymbol{w}_f = [\, \boldsymbol{f}_f^T \ \boldsymbol{M}_f^T \,]^T$. In the fixed reference frame $O_f - x_f y_f z_f$, the infinitesimal translational and rotational deformations of the moving platform caused by $\boldsymbol{w}_f$ are:

$$\boldsymbol{\Delta O_m} = \begin{bmatrix} \Delta x_{Om} & \Delta y_{Om} & \Delta z_{Om} & \Delta\theta_{xf} & \Delta\theta_{yf} & \Delta\theta_{zf} \end{bmatrix}^T \tag{42}$$

The input force and torque that are caused by actuations and constraints of the three subchains can be respectively expressed as:

$$\begin{cases} \boldsymbol{f_a} = [\|\boldsymbol{f_{1,a}}\| \quad \|\boldsymbol{f_{2,a}}\| \quad \|\boldsymbol{f_{3,a}}\|]^T \\ \boldsymbol{M_c} = [\|\boldsymbol{M_{1,c}}\| \quad \|\boldsymbol{M_{2,c}}\| \quad \|\boldsymbol{M_{3,c}}\|]^T \end{cases} \tag{43}$$

In accordance with the differential motions of the structure and the Jacobian of actuations and constraints, the output infinitesimal deformations of the moving platform can be, respectively, transformed as the input deformations of the actuators and the constrained subchains. Thus, the infinitesimal translational and rotational deformations of the actuators and of the constrained subchains are respectively deduced as:

$$\begin{cases} \boldsymbol{\Delta l} = [\Delta l_1 \quad \Delta l_2 \quad \Delta l_3]^T = (\boldsymbol{J_a}\nabla)\boldsymbol{\Delta O_m} \\ \boldsymbol{\Delta\varphi_c} = [\Delta\varphi_{1,c} \quad \Delta\varphi_{2,c} \quad \Delta\varphi_{3,c}]^T = (\boldsymbol{J_c}\nabla)\boldsymbol{\Delta O_m} \end{cases} \tag{44}$$

By applying the principle of virtual work to the overall structure, the relations of the input-output force and torque become:

$$\begin{aligned} \boldsymbol{w_f^T \Delta O_m} &= \boldsymbol{f_a^T \Delta l_a} + \boldsymbol{M_c^T \Delta\varphi_c} \\ &= \begin{bmatrix} \|\boldsymbol{f_{1,al}}\| \cos\phi_1 & \|\boldsymbol{f_{2,al}}\| \cos\phi_2 & \|\boldsymbol{f_{3,al}}\| \cos\phi_3 \end{bmatrix} \begin{bmatrix} \Delta l_1 \cos\phi_1 \\ \Delta l_2 \cos\phi_2 \\ \Delta l_3 \cos\phi_3 \end{bmatrix} + \boldsymbol{M_c^T \Delta\varphi_c} \\ &= \begin{bmatrix} \|\boldsymbol{f_{1,al}}\| & \|\boldsymbol{f_{2,al}}\| & \|\boldsymbol{f_{3,al}}\| \end{bmatrix} \begin{bmatrix} \cos^2\phi_1 & 0 & 0 \\ 0 & \cos^2\phi_2 & 0 \\ 0 & 0 & \cos^2\phi_3 \end{bmatrix} \begin{bmatrix} \Delta l_1 \\ \Delta l_2 \\ \Delta l_3 \end{bmatrix} + \boldsymbol{M_c^T \Delta\phi_c} \\ &= \boldsymbol{f_{al}^T} \begin{bmatrix} \cos^2\phi_1 & 0 & 0 \\ 0 & \cos^2\phi_2 & 0 \\ 0 & 0 & \cos^2\phi_3 \end{bmatrix} (\boldsymbol{J_a}\nabla)\, \boldsymbol{\Delta O_m} + \boldsymbol{M_c^T}\, (\boldsymbol{J_c}\nabla)\, \boldsymbol{\Delta O_m} \end{aligned} \tag{45}$$

namely:

$$\boldsymbol{w}_f = (\boldsymbol{J_a}\nabla)^T \begin{bmatrix} \cos^2\phi_1 & 0 & 0 \\ 0 & \cos^2\phi_2 & 0 \\ 0 & 0 & \cos^2\phi_3 \end{bmatrix} \boldsymbol{f_{al}} + (\boldsymbol{J_c}\nabla)^T\, \boldsymbol{M_c} \tag{46}$$

https://doi.org/10.1017/S0263574714001520 Published online by Cambridge University Press

where the input force $\boldsymbol{f_{al}}$ of the actuators and torque $\boldsymbol{M_c}$ of the constraints are respectively determined by the equivalent stiffness of the three subchains in Eqs. (39) and (40) as:

$$\begin{aligned}\boldsymbol{f_{al}} &= \left[\left\|\boldsymbol{f_{1,al}}\right\| \quad \left\|\boldsymbol{f_{2,al}}\right\| \quad \left\|\boldsymbol{f_{3,al}}\right\|\right]^T = \left[K_{1,al}\Delta l_1 \quad K_{2,al}\Delta l_2 \quad K_{3,al}\Delta l_3\right]^T \\ &= \begin{bmatrix} K_{1,al} & 0 & 0 \\ 0 & K_{2,al} & 0 \\ 0 & 0 & K_{3,al} \end{bmatrix} \begin{bmatrix} \Delta l_1 \\ \Delta l_2 \\ \Delta l_3 \end{bmatrix} = \begin{bmatrix} K_{1,al} & 0 & 0 \\ 0 & K_{2,al} & 0 \\ 0 & 0 & K_{3,al} \end{bmatrix} (\boldsymbol{J_a}\nabla)\,\boldsymbol{\Delta O_m} \end{aligned} \tag{47}$$

$$\begin{aligned}\boldsymbol{M_c} &= \left[\left\|\boldsymbol{M_{1,c}}\right\| \quad \left\|\boldsymbol{M_{2,c}}\right\| \quad \left\|\boldsymbol{M_{3,c}}\right\|\right]^T = \left[K_{1,c}\Delta\varphi_{1,c} \quad K_{2,c}\Delta\varphi_{2,c} \quad K_{3,c}\Delta\varphi_{3,c}\right]^T \\ &= \begin{bmatrix} K_{1,c} & 0 & 0 \\ 0 & K_{2,c} & 0 \\ 0 & 0 & K_{3,c} \end{bmatrix} \begin{bmatrix} \Delta\varphi_{1,c} \\ \Delta\varphi_{2,c} \\ \Delta\varphi_{3,c} \end{bmatrix} = \begin{bmatrix} K_{1,c} & 0 & 0 \\ 0 & K_{2,c} & 0 \\ 0 & 0 & K_{3,c} \end{bmatrix} (\boldsymbol{J_c}\nabla)\,\boldsymbol{\Delta O_m} \end{aligned} \tag{48}$$

By substituting Eq. (47) and (48) into Eq. (46), the output force and torque of the moving platform is obtained:

$$\begin{aligned}\boldsymbol{w}_f = (\boldsymbol{J_a}\nabla)^T &\begin{bmatrix} \cos^2\phi_1 & 0 & 0 \\ 0 & \cos^2\phi_2 & 0 \\ 0 & 0 & \cos^2\phi_3 \end{bmatrix} \begin{bmatrix} K_{1,al} & 0 & 0 \\ 0 & K_{2,al} & 0 \\ 0 & 0 & K_{3,al} \end{bmatrix} (\boldsymbol{J_a}\nabla)\,\boldsymbol{\Delta O_m} \\ (\boldsymbol{J_c}\nabla)^T &\begin{bmatrix} K_{1,c} & 0 & 0 \\ 0 & K_{2,c} & 0 \\ 0 & 0 & K_{3,c} \end{bmatrix} (\boldsymbol{J_c}\nabla)\,\boldsymbol{\Delta O_m} \end{aligned} \tag{49}$$

Thus, the 6×6 stiffness matrix of the Tri-pyramid Robot can be deduced from Eq. (49) and becomes:

$$\begin{aligned}\boldsymbol{K}_f = \frac{\boldsymbol{w}_f}{\boldsymbol{\Delta O_m}} &= (\boldsymbol{J_a}\nabla)^T\,\mathrm{diag}[\cos^2\phi_1,\ \cos^2\phi_2,\ \cos^2\phi_3]\mathrm{diag}\left[K_{1,al},\ K_{2,al},\ K_{3,al}\right](\boldsymbol{J_a}\nabla) \\ &+ (\boldsymbol{J_c}\nabla)^T\,\mathrm{diag}\left[K_{1,c},\ K_{2,c},\ K_{3,c}\right](\boldsymbol{J_c}\nabla) \end{aligned} \tag{50}$$

The stiffness matrix includes the effects of the actuations and constraints of the Tri-pyramid Robot, and the stiffness of all links, joints, actuators, fixed, and moving platforms are considered based on the analysis of the overall Jacobian matrix. The stiffness performance of the manipulator can now be evaluated based on this stiffness matrix.

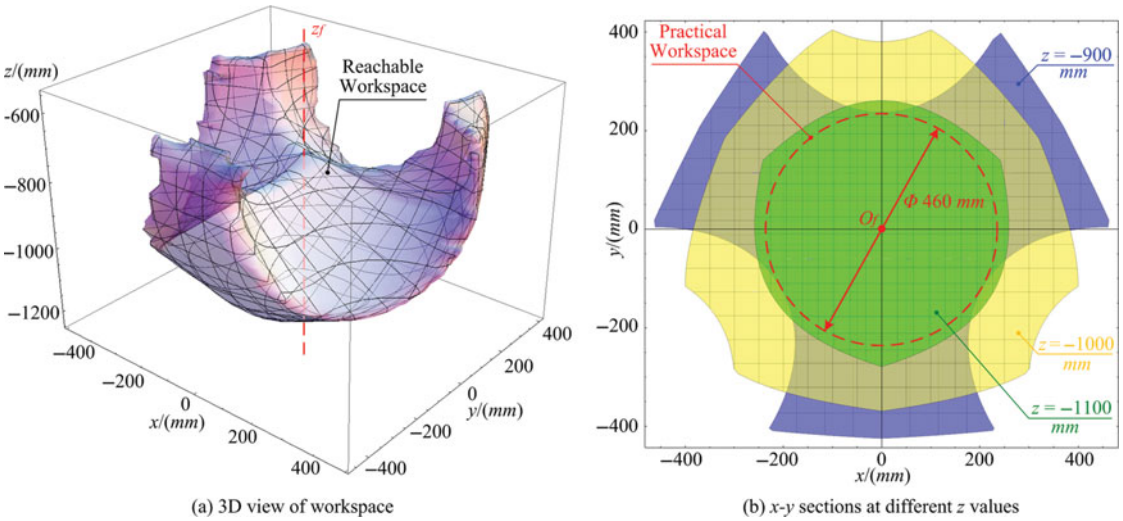
7. Workspace Evaluation

To evaluate the stiffness performance of the Tri-pyramid Robot, the reachable workspace should be determined and used to analyze the stiffness distributions. The shape and size of the reachable workspace is defined as the space that can be reached by the three translations of point O_m of the moving platform in the fixed reference frame $O_f - x_f y_f z_f$. The boundary of the reachable workspace is simultaneously constrained by the moving ranges, physical interference, and geometric constraints of all joints in the closed-loop form.

In accordance with Eq. (22), the rotational angles $\theta_{i,u}$ and $\theta_{i,d}$ of the two parallel revolute joints are equal as determined by the closed-loop constraint as:

$$\theta_{i,u} = -\theta_{i,d} = \arccos\left(\frac{\mathbf{s_{i,2}} \times \left[0 \quad 0 \quad -1\right]^T \times \mathbf{s_{i,2}} \cdot \overrightarrow{A_i C_i}}{\left\|\overrightarrow{A_i C_i}\right\|}\right) \tag{51}$$

https://doi.org/10.1017/S0263574714001520 Published online by Cambridge University Press



(a) 3D view of workspace

(b) x-y sections at different z values

Fig. 6. Workspace of the Tri-pyramid Robot.

where

$$\overrightarrow{A_iC_i} = \overrightarrow{O_fC_i} - \overrightarrow{O_fA_i} = \boldsymbol{r_O} + \overrightarrow{O_mC_i} - \boldsymbol{l_i} = \boldsymbol{r_O} + \boldsymbol{r_i} + \|\boldsymbol{h_i}\| \cos\gamma_i \begin{bmatrix} 1 & 1 & 1 \end{bmatrix}^T - \boldsymbol{l_i} \tag{52}$$

The translational displacements $\|\boldsymbol{l_i}\|$ ($P_{i,0}$) and $\|\boldsymbol{h_i}\|$ ($P_{i,1}$) are determined by the inverse position solution from Eqs. (6) and (4), respectively. Thus, by considering the moving ranges, physical interference, and geometric constraints of all joints, the corresponding constraint equations of the reachable workspace are given by:

$$\begin{cases} \|\boldsymbol{l_i}\|_{\min} \le \|\boldsymbol{l_i}\| \le \|\boldsymbol{l_i}\|_{\max} \\ \|\boldsymbol{h_i}\|_{\min} \le \|\boldsymbol{h_i}\| \le \|\boldsymbol{h_i}\|_{\max} \\ \theta_{i,\min} \le \theta_{i,u} = \left|\theta_{i,d}\right| \le \theta_{i,\max} \\ z < 0 \end{cases} \tag{53}$$

In order to determine the shape and size of the reachable workspace, a numerical search is performed based on Eq. (53). In the fixed reference frame $O_f - x_f y_f z_f$, if a point (x, y, z) satisfies the inequalities in Eq. (53), that point can be considered as part of the reachable workspace. Thus, by searching all points on each x-y section of $O_f - x_f y_f z_f$, a set of points is obtained. The three-dimensional (3D) arrangement of all these points constitutes the reachable workspace of the Tri-pyramid Robot.

The related values of the structural parameters and of the moving ranges of all joints for a Tri-pyramid Robot selected for illustrative purposes are listed in Table I. Based on the numerical search results in accordance to Eq. (53), the basic 3D shape and size of the reachable workspace is shown in Fig. 6(a). The shape of the reachable workspace is symmetric about the axis z_f. The coordinates of the extreme values of the reachable workspace are: $x \in [-457, 457]$, $y \in [-421, 402]$, and $z \in [-1262, -572]$ (the unit is mm). In Fig. 6(b), three x-y sections of the reachable workspace are generated. The three regions represent the x-y sections at $z = -1100$ mm, -1000 mm, and -900 mm, respectively. The three x-y sections have different shape and size. By considering the practical motion ranges of the moving platform and the general applications of the Tri-pyramid Robot, the practical workspace (namely, the sub-workspace of the reachable workspace) can be defined in a cylinder with a height of 200 mm (between the two x-y sections at the $z = -1100$ mm and -900 mm), where the maximal diameter of the cylinder is $\Phi = 460$ mm (around the center point O_f). The stiffness and its distributions throughout the practical workspace of the Tri-pyramid Robot will be discussed in the next section.

https://doi.org/10.1017/S0263574714001520 Published online by Cambridge University Press

Table I. Structural parameters of the Tri-pyramid Robot.

Parameter	Value	Parameter	Value
α_1	90°	$\|\boldsymbol{l_i}\|_{\min}$	400 mm
α_2	210°	$\|\boldsymbol{l_i}\|_{\max}$	1250 mm
α_3	330°	$\|\boldsymbol{h_i}\|_{\min}$	600 mm
α_{Pi}	−35°	$\|\boldsymbol{h_i}\|_{\max}$	1200 mm
α_{Ri}	−35°	$\theta_{i,\min}$	−90°
γ_i	−30°	$\theta_{i,\max}$	90°
$\|\boldsymbol{r_i}\|$	100 mm		

Table II. Physical parameters of the Tri-pyramid Robot.

Parameter	Value	Parameter	Value
$K_{i,\alpha a}$	2.5×10^9Nmm/rad	$I_{ik,GOf}$	4.22×10^4 mm^4
$L_{i,a}$	6.5 mm	$I_{ik,AH}$	2.53×10^4 mm^4
$d_{i,a}$	31.5 mm	$I_{ik,HH}$	3.21×10^4 mm^4
$\alpha_{i,t}$	14.5°	$I_{ik,HB}$	2.36×10^4 mm^4
$\mu_{i,c}$	0.2	$I_{ik,BOm}$	1.78×10^4 mm^4
E	2.03×10^5Mpa	$\|\boldsymbol{h_{i,u}}\|$	600 mm
		$\|\boldsymbol{h_{i,d}}\|$	400 mm

8. Stiffness Evaluation

In the structure of the Tri-pyramid Robot, the stiffness matrix is varied when the moving platform is moving to different positions. In addition, the output stiffness is also dependent on the direction of the applied external loads on the moving platform. In the reachable workspace, the minimal stiffness should be larger than a designed value to ensure accuracy of manipulation. Thus, the distribution of the stiffness should be evaluated in the reachable workspace.

Each point of the reachable workspace is characterized by a minimal and maximal value of the stiffness. The actual output stiffness at each point depends on the direction of the external load. The range of the values can be characterized by the minimal and maximal eigenvalues of the stiffness matrix, because the output stiffness in an arbitrary direction is bounded by the minimal and maximal eigenvalues of the stiffness matrix in a given pose.[17] The variations of the minimal and maximal eigenvalues can be used as stiffness performance indices to evaluate the stiffness distribution in the reachable workspace.

By substituting all coordinates of the reachable workspace into the stiffness matrix in Eq. (50), the distributions of the minimal and maximal eigenvalues of the stiffness matrix can be respectively determined in the fixed reference frame $O_f - x_f y_f z_f$. The structural and physical parameters are listed in Tables I and II, respectively.

In Fig. 7, $K_{f\max}$ and $K_{f\min}$ represent the maximal and minimal eigenvalues of the stiffness matrix. The distributions of $K_{f\max}$ and $K_{f\min}$ are analyzed, as an example, in three x-y sections ($z = -900$, -1000, and $-1100mm$), respectively. The shape of the distributions is symmetric about the axis z. The maximal eigenvalues are increased from the center outward, and increased along the positive direction of axis z. From the center outward, the minimal eigenvalues are decreased, and then increased. In each x-y section, the inner part of decreased minimal eigenvalues are decreased along the positive direction of axis z, while the outward part of increased minimal eigenvalues are increased along the positive direction of axis z. Thus, by assuming that the minimal eigenvalue of the stiffness matrix is 1.4×10^{10}, the maximal stiffness workspace can be determined as a cylinder with a maximal diameter of $\Phi = 410$ mm (around the center point O_f) and height 200 mm (between the two x-y sections at the $z = -900$ mm and -1100 mm) as shown in Fig. 7(d), which is a sub-workspace of the practical workspace.

Among all the basic structural constants α_i, α_{Pi}, α_{Ri}, γ_i, $\|\boldsymbol{r_i}\|$, $\|\boldsymbol{h_{i,u}}\|$, and $\|\boldsymbol{h_{i,d}}\|$, α_i determines the symmetric property of the structure and workspace, while the variations of $\|\boldsymbol{r_i}\|$, $\|\boldsymbol{h_{i,u}}\|$, and $\|\boldsymbol{h_{i,d}}\|$ can change the size of the workspace (instead of the shape of the workspace), because the different lengths of $\|\boldsymbol{r_i}\|$, $\|\boldsymbol{h_{i,u}}\|$, and $\|\boldsymbol{h_{i,d}}\|$ have no influence on the constraint angles between the

https://doi.org/10.1017/S0263574714001520 Published online by Cambridge University Press

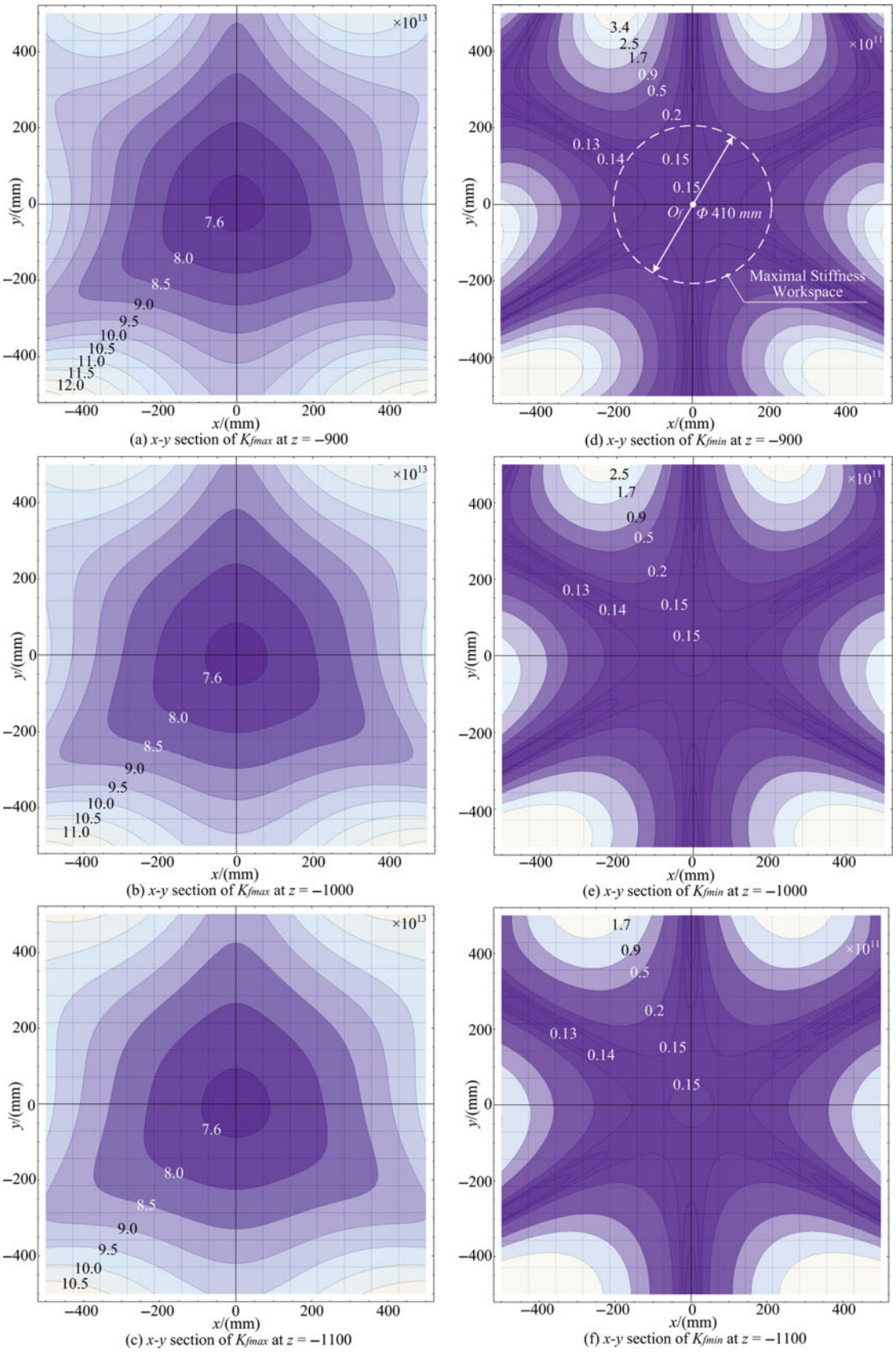


Fig. 7. Distributions of max/min eigenvalues of the stiffness matrix at different x-y sections.

https://doi.org/10.1017/S0263574714001520 Published online by Cambridge University Press

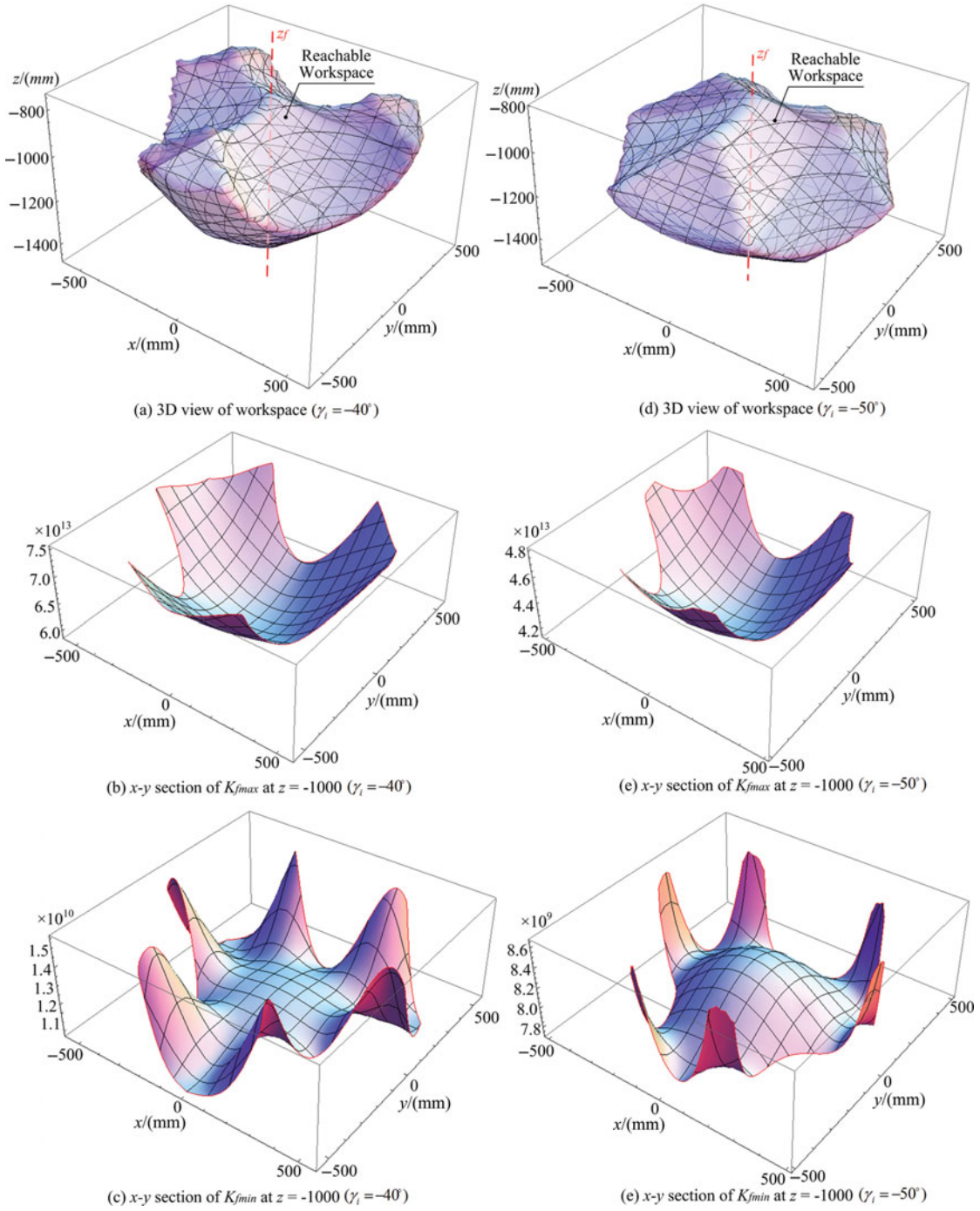


Fig. 8. The workspace and stiffness distributions for different values of γ_i.

axes of all of the joints. In the three subchains, the intersection angles α_{Pi}, α_{Ri}, and γ_i determine the constraint relations between all of the joints. Different constraint angles of the joints induce different shapes and sizes of the structure and of the workspace. In the illustrative example of a simplified sensitivity analysis of the structural parameters and of a simplified structural optimization, to be presented below, only the variation of γ_i will be considered while assuming that the other variables are constants.

During the linear actuation of $P_{i,0}$, in order to actuate the passive motion of joint $P_{i,1}$, joint $P_{i,1}$ cannot be parallel or perpendicular to $P_{i,0}$. Thus, the variation range of the intersection angle is $\gamma_i \in (0°, -((\pi/2) - |\alpha_{Ri}|))$. In Figs. 6 and 7, the workspace and the distributions of the stiffness are

https://doi.org/10.1017/S0263574714001520 Published online by Cambridge University Press

generated for γ_i equal to -30°. In order to evaluate the variations of the workspace and the stiffness distributions by different values of γ_i, results of a numerical search are shown in Fig. 8., for $\gamma_i = -40^\circ$ and -50°. Compared to the workspace shown in Fig. 6, the sizes of the workspaces have increased in Fig. 8. Evidently, the maximal and minimal eigenvalues of the stiffness are decreased with an increase of γ_i. Thus, by evaluating the workspace and distributions of the maximal and minimal eigenvalues as a function of γ_i, it can be shown that the maximal size of the practical workspace is achieved when $\gamma_i = -42.5^\circ$. The maximal diameter of the cylinder of the practical workspace, in this case, is $\Phi = 540$ mm with a height of 230 mm between two x-y sections at $z = -1050$ mm and -1280 mm. Correspondingly, the maximal stiffness workspace can be defined as a sub-workspace of the practical workspace with a maximal diameter of $\Phi = 450$ mm and height of 230 mm when the minimal eigenvalue of the stiffness matrix is 1.1×10^{10}.

9. Conclusions

The motions and constraints of a 3-DOF TPM (the Tri-pyramid Robot) are analyzed. There are only four 1-DOF joints required in each subchain. A small size of the moving platform and fixed linear actuations are designed for achieving a better kinematic characteristic. The inverse position solution was obtained in the closed-loop constraint analysis. By considering the 6-DOF deformations of the moving platform, a 6×6 overall Jacobian matrix of the Tri-pyramid Robot was built based on the theory of reciprocal screws, which includes the constraint and actuation effects on the output stiffness.

In accordance with the overall Jacobian matrix method, the stiffness model of the Tri-pyramid Robot was established. The model includes the deformations of all links, joints, actuators, fixed, and moving platforms. In each subchain, one torsional spring and five bending springs were used to represent the equivalent spring structure of the stiffness model. A 6×6 output stiffness matrix was obtained by the transformations of loads and deformations in the closed-loop form. Furthermore, the stiffness performance of the Tri-pyramid Robot was characterized and evaluated by the maximal and minimal eigenvalues of the stiffness matrix in the reachable workspace. By evaluating the workspace and distributions of the maximal and minimal eigenvalues with the variation of structural parameters, the maximal size of the practical workspace was analyzed, and the maximal stiffness workspace can be determined according to the stiffness distributions. The stiffness model and analysis provide the basic constraints for the parametric design of the Tri-pyramid Robot.

Acknowledgements

The authors would like to acknowledge the support of the Department of Energy, USA DE-EE0005764 for their support.

References

1. R. Clavel, "DELTA, A Fast Robot with Parallel Geometry," *18th International Symposium on Industrial Robots*, Sydney, Australia 91–100 (1988).
2. R. Clavel, "Device for the Movement and Positioning of an Element in Space," United States Patent No. 4,976,582 (1990).
3. L. W. Tsai, G. C. Walsh and R. E. Stamper, "Kinematics of a Novel Three DoF Translational Platform," *IEEE International Conference on Robotics and Automation*, Minneapolis, MN 3446–3451 (1996).
4. L. W. Tsai and S. Joshi, "Kinematics and optimization of a spatial 3-UPU parallel manipulator," *ASME, J. Mech. Des.* **122**, 439–446 (2000).
5. B. Siciliano, "The tricept robot: inverse kinematics, manipulability analysis and closed-loop direct kinematics algorithm," *Robotica* **17**, 437–455 (1999).
6. D. Zhang and C. M. Gosselin, "Kinetostatic analysis and design optimization of the tricept machine tool family," *ASME J. Manuf. Sci. Eng.* **124**, 725–733 (2002).
7. K. E. Neumann, "Next Generation Tricept—A True Revolution in Parallel Kinematics," *Proceedings of the 4th Chemnitz Parallel Kinematics Seminar*, Zwickau, Germany (2004) pp. 591–594.
8. J. M. Hervé and F. Sparacino, "Structural Synthesis of Parallel Robots Generating Spatial Translation," *Proceedings of the 5th International Conference on Advanced Robotics*, Pisa, Italy **1** (1991) pp. 808–813.
9. X. Kong and C. M. Gosselin, "Kinematics and singularity analysis of a novel type of 3-CRR 3-DOF translational parallel manipulator," *Int. J. Robot. Res.* **21**, 791–798 (2002).
10. M. Carricato and V. Parenti-Castelli, "Singularity-free fully-isotropic translational parallel mechanisms," *Int. J. Robot. Res.* **21**, 161–174 (2002).
11. H. S. Kim and L. W. Tsai, "Design optimization of a cartesian parallel manipulator," *ASME, J. Mech. Des.* **125**, 43–51 (2003).

https://doi.org/10.1017/S0263574714001520 Published online by Cambridge University Press

12. C. C. Lee and J. M. Hervé, "Cartesian parallel manipulators with pseudoplanar limbs," *ASME, J. Mech. Des.* **129**, 1256–1264 (2007).
13. G. Gogu, "Structural synthesis of fully-isotropic translational parallel robots via theory of linear transformations," *Eur. J. Mech.* **23**, 1021–1039 (2004).
14. X. Kong and C. M. Gosselin, "Type synthesis of 3-DOF translational parallel manipulators based on screw theory," *J. Mech. Des.* **126**, 83–92 (2004).
15. C. M. Gosselin, "Stiffness mapping for a parallel manipulators," *IEEE Trans. Robot. Autom.* **6**, 377–382 (1990).
16. C. M. Gosselin and D. Zhang, "Stiffness analysis of parallel mechanisms using a lumped model," *Int. J. Robot. Autom.* **17**, 17–27 (2002).
17. B. S. El-Khasawneh and P. M. Ferreira, "Computation of stiffness and stiffness bounds for parallel link manipulators," *Int. J. Mach. Tools Manuf.* **39**, 321–342 (1999).
18. M. Ceccarelli and G. Carbone, "A stiffness analysis for CaPaMan (Cassino Parallel Manipulator)," *Mech. Mach. Theory* **37**, 427–439 (2002).
19. T. Huang, X. Zhao and D. J. Whitehouse, "Stiffness estimation of a tripod-based parallel kinematic machine," *IEEE Transactions on Robotics and Automation* **18**, 50–58 (2002).
20. F. Xi, D. Zhang, C. M. Mechefske and S. Y. T. Lang, "Global kinetostatic modeling of tripod-based parallel kinematic machine," *Mech. Mach. Theory* **39**, 357–377 (2004).
21. D. Zhang and S. Y. T. Lang, "Stiffness modeling for a class of reconfigurable PKMs with three to five degrees of freedom," *J. Manuf. Syst.* **23**, 316–327 (2004).
22. H. H. Pham and I. M. Chen, "Stiffness modeling of flexure parallel mechanism," *Precis. Eng.* **29**, 467–478 (2005).
23. F. Majou, C. M. Gosselin, P. Wenger and D. Chablat, "Parametric stiffness analysis of the Orthoglide," *Mech. Mach. Theory* **42**, 296–311 (2007).
24. J. Chen and F. Lan, "Instantaneous stiffness analysis and simulation for hexapod machines," *Simul. Modelling Pract. Theory* **16**, 419–428 (2008).
25. H. K. Jung, C. D. Crane III and R. G. Roberts, "Stiffness mapping of compliant parallel mechanisms in a serial arrangement," *Mech. Mach. Theory* **43**, 271–284 (2008).
26. A. Pashkevich, D. Chablat and P. Wenger, "Stiffness analysis of overconstrained parallel manipulators," *Mech. Mach. Theory* **44**, 966–982 (2009).
27. J. Wu, J. Wang, L. Wang, T. Li and Z. You, "Study on the stiffness of a 5-DOF hybrid machine tool with actuation redundancy," *Mech. Mach. Theory* **44**, 289–305 (2009).
28. Y. Shneor and V. T. Portman, "Stiffness of 5-axis machines with serial, parallel, and hybrid kinematics: Evaluation and comparison," *CIRP Ann. - Manuf. Technol.* **59**, 409–412 (2010).
29. A. Pashkevich, A. Klimchik and D. Chablat, "Enhanced stiffness modeling of manipulators with passive joints," *Mech. Mach. Theory* **46**, 662–679 (2011).
30. B. Hua, Y. Lu, Q. Tan, J. Yu and J. Han, "Analysis of stiffness and elastic deformation of a 2(SP+SPR+SPU) serial–parallel manipulator," *Robot. Comput.-Integr. Manuf.* **27**, 418–25 (2011).
31. A. Rezaei, A. Akbarzadeh and M. R. Akbarzadeh-T, "An investigation on stiffness of a 3-PSP spatial parallel mechanism with flexible moving platform using invariant form," *Mech. Mach. Theory* **51**, 195–216 (2012).
32. J. Aginaga, I. Zabalza, O. Altuzarra and J. Najera, "Improving static stiffness of the 6-RUS parallel manipulator using inverse singularities," *Robot. Comput.-Integr. Manuf.* **28**, 458–471 (2012).
33. V. T. Portman, V. S. Chapsky and Y. Shneor, "Workspace of parallel kinematics machines with minimum stiffness limits: Collinear stiffness value based approach," *Mech. Mach. Theory* **49**, 67–86 (2012).
34. D. M. Gan, J. S. Dai, J. Dias and L. D. Seneviratne, "Unified Kinematics and Singularity Analysis of A Metamorphic Parallel Mechanism with Bifurcated Motion," *ASME, J. Mech. Robot.* **5**, 041104 (2013).
35. D. M. Gan, Q. Z. Liao, J. S. Dai and S. M. Wei, "Design and kinematics analysis of a new 3CCC parallel mechanism," *Robotica* **28**, 1065–1072 (2010).
36. M. A. Hosseini and H. M. Daniali, "Weighted local conditioning index of a positioning and orienting parallel manipulator," *Scientica Iranica B* **18**, 115–120 (2011).
37. Y. Li and Q. Xu, "Stiffness analysis for a 3-PUU parallel kinematic machine," *Mech. Mach. Theory* **43**, 186–200 (2008).
38. Q. Xu and Y. Li, "An investigation on mobility and stiffness of a 3-DOF translational parallel manipulator via screw theory," *Robot. Comput.-Integr. Manuf.* **24**, 402–414 (2008).
39. Y. Wang, H. Liu, T. Huang and D. G. Chetwynd, "Stiffness modeling of the tricept robot using the overall jacobian matrix," *ASME, J. Mech. Robot.* **1**, 021002 (2009).
40. S. A. Joshi and L. W. Tsai, "Jacobian analysis of limited-DOF parallel manipulators," *ASME, J. Mech. Des.* **124**, 254–258 (2002).
41. R. S. Ball, *A Treatise on the Theory of Screws* (Cambridge University Press, Cambridge, 1900).
42. K. H. Hunt, *Kinematic Geometry of Mechanisms* (Clarendon Press, Oxford, 1978).
43. J. M. Hervé, "The Lie group of rigid body displacements, a fundamental tool for mechanism design," *Mech. Mach. Theory* **34**, 719–730 (1999).
44. P. Fanghella and C. Galletti, "Metric relations and displacement groups in mechanism and robot kinematics," *ASME, J. Mech. Des.* **117**, 470–478 (1995).

https://doi.org/10.1017/S0263574714001520 Published online by Cambridge University Press